buildings

MDPI

Article

Enhanced Modal Participation Ratio-Based Structural Damage Identification: A New Filtering Approach Using Modal Assurance Criteria

Zafer Yilmaz [1], Fatih Yesevi Okur [2,3], Murat Günaydin [2,3] and Ahmet Can Altunişik [2,3,*]

[1] Civil and Environmental Engineering, UCLA Samueli School of Engineering, Los Angeles, CA 90095, USA; zafer@ucla.edu
[2] Department of Civil Engineering, Karadeniz Technical University, Trabzon 61080, Türkiye; yesevi@ktu.edu.tr (F.Y.O.); muratgunaydin@ktu.edu.tr (M.G.)
[3] Earthquake and Structural Health Monitoring Research Center, Karadeniz Technical University, Trabzon 61080, Türkiye
* Correspondence: ahmetcan@ktu.edu.tr

Abstract: The interest in damage identification methods has increased significantly in recent years due to the rising demand for structural health monitoring of structures. This study presents an enhanced version and validation of a recently introduced method for damage detection, localization and quantifying damage using vibration data. The method is validated through a building application, a scaled steel frame model built in the laboratory. The validation is carried out using eight different damage scenarios in numerical and experimental studies. These studies are based on finite element analysis and ambient vibration tests. A newly introduced filtering approach that utilizes MAC rejection levels in Modal Participation Ratio derivation is provided to replace the user-controlled bandpass filter to obtain more reliable vibration data in experimental investigations. The results showed that the proposed procedure is more capable of correctly detecting, localizing and quantifying damage to a building, considering the real-life conditions.

Keywords: damage detection; damage identification; modal participation ratio; ambient vibration test; finite element model; dynamic characteristics

check for updates

Citation: Yilmaz, Z.; Okur, F.Y.; Günaydin, M.; Altunişik, A.C. Enhanced Modal Participation Ratio-Based Structural Damage Identification: A New Filtering Approach Using Modal Assurance Criteria. *Buildings* **2023**, *13*, 2467. https://doi.org/10.3390/buildings13102467

Academic Editors: Andrea Benedetti and André Furtado

Received: 9 June 2023
Revised: 18 August 2023
Accepted: 25 September 2023
Published: 28 September 2023

Copyright: © 2023 by the authors. Licensee MDPI, Basel, Switzerland. This article is an open access article distributed under the terms and conditions of the Creative Commons Attribution (CC BY) license (https://creativecommons.org/licenses/by/4.0/).

1. Introduction

It is crucial to correctly determine and solve problems and inadequacies concerning human life. Using advanced technology accelerated the process and helped solve many complex problems. By using modern technologies and making use of extensive knowledge, new methods have been developed for various problems. For engineers, damage identification has been one of the main concerns regarding human life. Various methods have been developed to perform effective damage identification. It is necessary to extensively evaluate the developed methods before using them, and there are various ways to assess a method. Numerical tests and simulations on computers have been used lately as initial tests. However, there is a limit to simulating perfect site conditions in numerical tests. Therefore, experimental tests, despite being more complicated and expensive, are a better source of information. Furthermore, utilizing both numerical and experimental studies in method testing produces the best outcome, since the quickness and cost effectiveness of numerical study can be used to avoid economic and time loss in the experimental process.

Damage identification using dynamic characteristics is frequently studied by researchers to create effective methods to be used in the field. Dynamic characteristics were an alternative replacement for the preliminary destructive and non-destructive damage detection methods. Some of the fundamental dynamic characteristics, such as natural frequency, mode shape and damping ratio, were monitored through non-destructive tests. The changes in these values through time or under the influence of an external effect were used

for damage identification and health monitoring of structures. Scientists practiced many tests on different structure types with different damage patterns in different environmental conditions to create a method that can be used in real-life situations. The earliest dynamic characteristic-based system and damage identification studies focused on natural frequency, mode shape and damping ratio. Vandier [1] studied the natural frequency variations to ease the process of damage detection below the waterline. Natural frequencies were sensitive to the removal of structural members on a computer model of an offshore platform. Adams et al. [2] performed experimental tests on one-dimensional bar elements, where they examined damage through natural frequency changes. The authors stated that the method presented the possibility for effective and quick detection, localization and quantification of damage based on different contributions of localized damages in each mode due to the structure's non-uniform stress distribution. Also, taking account of natural frequencies, studies on damage identification were frequently carried out [3–5]. Rizos et al. [6] studied variations in the mode shapes of the beam under uniformly extending transverse surface cracks. Analytical solutions and amplitude measurements were used, and the effect of the crack on the mode shapes of the beam was examined for the five different damage locations with four different crack depths. The location and depth of the moderate cracks (more than 10% of the width) were effectively obtained. However, due to low sensitivity, cracks smaller than 10% of the width of the beam could not be identified. Stubbs et al. [7] produced a damage detection study on an I-40 bridge by creating a validated Finite Element (FE) model of the beam. Modal frequencies and mode shapes of the pre-damage and post-damage states of the bridge were determined using modal analysis to evaluate the damage localization of the method in a full-scale structure. Using only the data from three modes, the accurate location of damage was determined. Several more studies were reported on damage identification methods which are built on natural frequencies and mode shapes [8–12]. Razak and Choi [13] studied the natural frequency and damping ratio changes in concrete beams exposed to corrosion. Modal and load tests were performed on two corroded concrete beams with moderate cracking and very slight spalling. Natural frequencies and load-carrying capacity of a beam with very slight spalling decreased more compared to a reference beam and a beam with a moderate crack. The damping ratio changes in the first mode were deemed inconsistent by the authors. However, the damping ratios of the second and third modes were found to have a consistent trend with severity increase. Moreover, many more methods, which are built on dynamic characteristics, were examined using different structure types and damage patterns [14–22].

Pandey and Biswas [23] investigated the changes in the flexibility matrix for damage identification using a numerical beam model and experimental data collected from a wide-flange steel beam. The method was found effective for finding damage to sections with a high bending moment. Liew and Wang [24] presented a method that uses the wavelet theory for crack identification. Damage detection through eigenvalue changes and wavelet method was compared on a mathematical model of a simply supported cracked beam. Damage identification via the wavelet method was found easier than traditional eigenvalue analysis. Abrupt changes for the eigenvalues were obtained at higher-order modes, where the results were mostly inaccurate. Mehrjoo et al. [25] presented a method of damage intensity estimation for truss bridge structures using a back-propagation-based neural network. A Multi-Layer Perceptron (MLP), which is the most used neural network for structural identification problems, was employed. The natural frequencies and mode shapes derived from numerical models of a simple truss and the Louisville Bridge truss were employed in the neural network. It was found that the location and severity of damage in truss bridge joints were predicted with high accuracy. Also, MLP network architecture was found to be effective for damage location and severity determination. Pawar et al. [26] proposed a method of damage detection created with the integration of Spatial Fourier Analysis and Artificial Neural Networks. Fourier coefficients of the mode shapes derived from mode shapes of the FE model by using spatial Fourier series were found to be sensitive to both damage size and location. A damage index was formulated and employed in a

neural network that was trained to detect damage. The trained and developed neural network was successful at finding the damage location and size. The method proved to be effective for automated damage detection. Huang et al. [27] proposed a nondestructive method based on a generic algorithm to identify the location and severity of the damage while taking varying temperature and noise effects into account.

In addition to development of new methods, many studies are performed by testing these methods to determine the dynamic response of unique structures [28–31]. With advancements in both literature and the technology, damage identification methods using neural networks, algorithms and hybrids of many different methods have been developed [32–36].

However, studies on extracting relatively simple parameters representing dynamic characteristics of a structure are still taking place in the field. This study aimed to investigate and enhance one of these parameters. Mehboob et al. [37] proposed a method utilizing modal contributions for each mode and the eigenvalues to create an index value. This index was appreciated to be more feasible for damage detection in beams. Furthermore, a recently introduced damage detection method was proposed by Park and Oh [38] and Park et al. [39]. A new index called the modal participation ratio (MPR) was identified for the damage detection of the building structures. The MPR value is the representative value of the modal response extracted from dynamic responses measured in non-destructive testing such as ambient vibration tests. The various damage scenarios were evaluated taking account of relationship between the MPR, representing a modal contribution for a specific mode and degree of freedom in buildings, and the story stiffness damage factor. It was concluded that the approach promised a potential for broad-scale damage identification and localization. To our knowledge, investigation into the damage identification using MPR values is rare, and should be supported by numerical and experimental studies. The contribution of this study may assist in alleviating this situation.

In this study, a recently introduced damage detection method was evaluated with the aim of determining the efficiency of the method. The study included the following steps:

- ✓ Determining the dynamic response of the building model investigated using a numerical method;
- ✓ Conducting an experimental test to obtain the dynamic responses and characteristics of a model;
- ✓ Calculating the MPR values in light of numerical and experimental data;
- ✓ Comparing numerical and experimental test results;
- ✓ Developing a new filtering approach to get rid of user effects on MPR derivation;
- ✓ Evaluating the damage detection method in case of using a new filtering approach for experimental data.

2. Methodology

2.1. Dynamic Response

One of the ways to obtain a dynamic response is through processing transient analysis results. In this case, artificial vibrations are applied to the numerical model to simulate ambient vibrations caused by environmental effects. Then, the dynamic responses of the building to these excitations are collected (Figure 1). Ambient excitations can be simulated with randomized white noise acceleration. The time-step and total length of the white noise acceleration are significant for the accurate modal response. The time-step value and duration of white noise acceleration need to be determined by foreseeing the highest possible frequency value to be considered based on the studied structure [40].

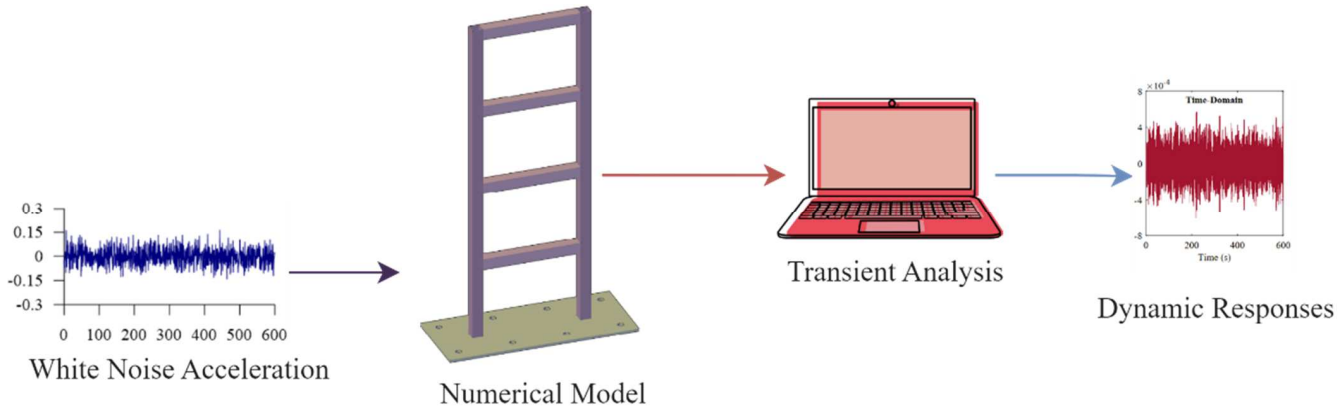


Figure 1. Flow chart of dynamic response extraction through transient analysis.

Operational Modal Analysis (OMA), also known as the output-only ambient vibration method, is a vibration-based non-destructive structural health monitoring method that has been widely used in the field of civil engineering in recent years. The method is employed to obtain dynamic characteristics such as natural frequency, mode shapes and damping ratios. This also provides valuable information for assessment of the current structural behavior of the building. Within the scope of this method, sensitive accelerometers are placed on the structure, considering the geometry and degrees of freedom of the structures. Then, vibration signals obtained are transferred to data acquisition unit and dynamic responses are available to use after signal processing in up-to-date software (Figure 2).

The dynamic characteristics of the structure are determined using algorithms in the frequency or time domain because the amplitude of the vibrations acting on the structure and their variation with time are unknown. In the study, to extract the dynamic characteristics, the Enhanced Frequency Domain Decomposition (EFDD) method was employed. More information about algorithms is available in the literature [41,42].

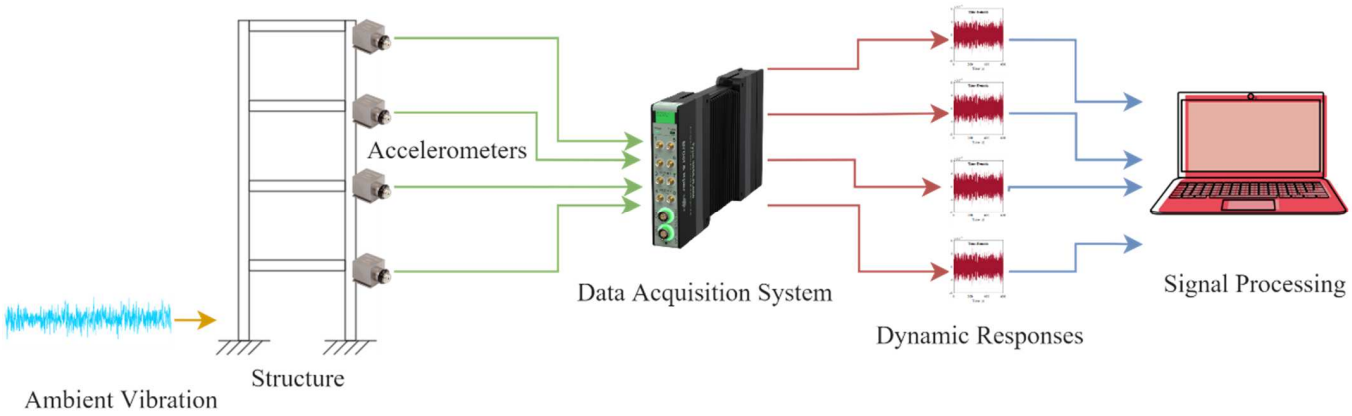


Figure 2. Flow chart of dynamic response extraction using OMA.

2.2. Modal Participation Ratio (MPR) Derivation

MPR derivation is performed using the dynamic responses obtained by transient analysis and OMA. Unlike the modal participation mass ratio, MPR represents the contribution of each measurement point or degrees of freedom and each mode. It creates an opportunity to detect structural damage between measurement points or DOFs. However, the filtering procedure should be employed in the Fast Fourier Transform (FFT) procedure to separate the dynamic response of each measurement point to considered number of modes. A more detailed and visually aided explanation of MPR derivations is presented in Yilmaz (2022) [43]. First, the dynamic response of j-th measurement point $u^j(t)$ is converted to frequency domain data of j-th measurement point $U^j(f)$ using FFT, as shown

in Equation (1). FFT is repeated as many times as the number of measurement points or DOF (n_d).

$$U^j(f) = \int_{-\infty}^{\infty} u^j(t) e^{-i\omega t} dt, j = 1 \; to \; n_d \tag{1}$$

2.2.1. Filtering

After transforming the time domain data of each measurement point to the frequency domain, filtering was performed to divide the frequency domain into the number of considered modes n_m and to form frequency domain data for each mode.

Bandpass Filtering

The filtering value R_b used for bandpass filtering is calculated using Equation (2), where f_1 is the first natural frequency, R_i is the difference between two adjacent mode frequencies, and n_m is the number of considered modes [44]. The smallest value of differences between adjacent mode frequencies and two times the value of the first natural frequency was selected. Then, this value is multiplied by user-defined γ value that helps adjust the filtering interval with a varying value of 0 to 1. Depending on the length of the data, the filtering coefficient γ can be decreased to reduce computational time and avoid noise effect. However, frequency domain data needs to be graphed and detailed to avoid filtering out the peak values within the original range formed by the maximum value of the filtering coefficient. For a numerical study within this research, γ is assumed to be one since it is a computer model, and the environmental effects are non-existent. This coefficient is highly effective in experimental research. Therefore, a method of filtering using the MAC rejection is introduced later to eliminate this drawback.

$$R_b = \gamma \times min\{2 \times f_1, R_i\}, \;\; i = 1 \; to \; n_m \tag{2}$$

The frequency domain data of each measurement point are divided into modes using the R_b value, as shown in Equation (3), where f_i represents the natural frequency value of i-th mode and f_i^r is the natural frequency value within the filtering range. From this, the frequency domain data of each measurement point filtered for each mode $U_i^j(f)$ are obtained.

$$U_i^j(f) = U^j(f_i^r), \quad i = 1 \; to \; n_m, \;\; f_i - \frac{R_b}{2} \leq f_i^r \leq f_i + \frac{R_b}{2} \tag{3}$$

MAC Rejection Level

Bandpass filtering is a convenient method for numerical studies. However, measurements of experimental studies contain more noise data compared to numerical studies. Therefore, a method of filtering through the MAC rejection level was developed for an automated and more reliable derivation of MPR values in experimental studies rather than using user-defined filtering values, as shown in bandpass filtering. The MAC rejection level varies between 0 and 1, and the value describes the degree of correlation between the two modes. Both sides of the selected peak value were searched for correlation, and an interval was determined based on the MAC rejection level [45,46]. Figure 3 shows the singular values of spectral densities of the test setup for the undamaged case. In addition, the interval formed by the 0.9 MAC rejection level on one of the SVD lines for first mode is highlighted in red. The undamaged A lower rejection level means that less correlation is required, resulting in a wider interval [47].

Figure 4 shows the intervals formed by different MAC rejection levels. It should be stated that the distances to the right and left from frequency values were uneven. Therefore, distance to the closest limit is applied to the other side to obtain symmetrical filtering. It should be highlighted that symmetrical filtering showed better results when compared to the ΔMPR obtained with unsymmetrical filtering.

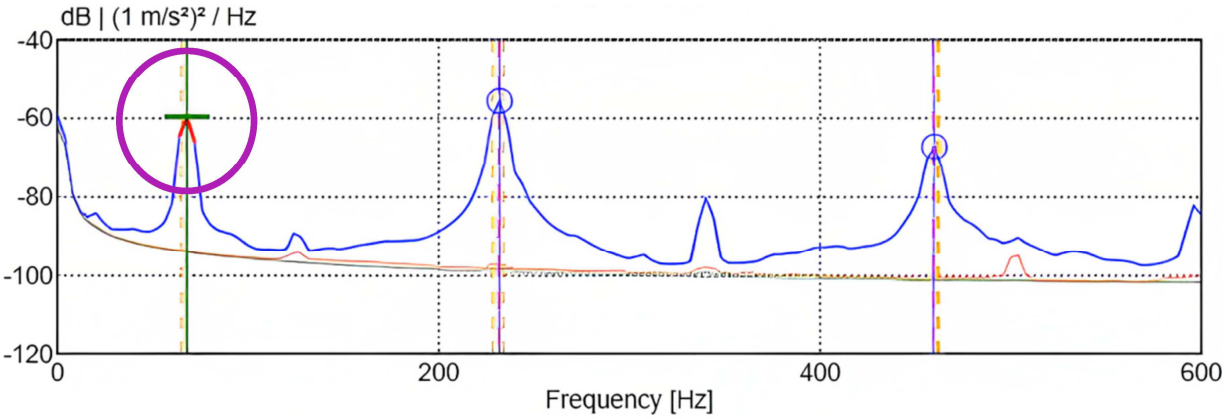


Figure 3. Interval of 0.9 MAC rejection level on singular values of spectral densities.

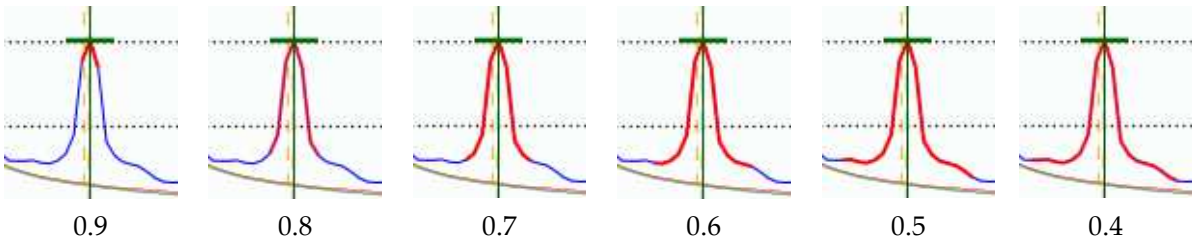


Figure 4. Intervals formed by different MAC rejection levels.

Equation (4) shows the calculation of filtering value x_l, where $x_{i(min)}$ and $x_{i(max)}$ denote the start and the end values of interval for a specific MAC rejection level. The calculation is repeated as many times as the number of modes considered (n_m).

$$x_l = min\left\{\frac{f_i - x_{i(min)}}{f_i}, \frac{x_{i(max)} - f_i}{f_i}\right\}, \quad i = 1 \; to \; n_m \tag{4}$$

The frequency domain data of each measurement point is divided into modes using Equation (5). From this, frequency domain data of each measurement point for each mode $U_i^j(f)$ is obtained. Equation (5) is similar to Equation (3); however, these formulas differ by the parameter utilized for filtering margins.

$$U_i^j(f) = U^j(f_i^r), \;\; i = 1 \; to \; n_m, \;\; f_i \times (1 - x_l) \le f_i^r \le f_i \times (1 + x_l) \tag{5}$$

2.3. MPR Variation

The inverse FFT is applied, and the modal response of each measurement point (or DOF) and mode $y_i^j(f)$ is extracted using Equation (6).

$$y_i^j(t) = \frac{1}{2\pi}\int_{-\infty}^{\infty} U_i^j(f) e^{ift} df, \;\; i = 1 \; to \; n_m, \;\; j = 1 \; to \; n_d \tag{6}$$

To obtain the MPR value of each measurement point (or DOF) and mode combination, the root means square of modal response ($MRRMS_i^j$) for each measurement point and mode combination were separately calculated using Equation (7).

$$MRRMS_i^j = \sqrt{\frac{\sum_{x=1}^{l} u_i^j(x)^2}{l}}, \;\; i = 1 \; to \; n_m, \;\; j = 1 \; to \; n_d \tag{7}$$

where summation of squares of each modal response of i-th mode and j-th measurement point is divided by l, which is the data length of the same modal response.

The MPR value is the ratio of the root mean square of modal response for *i*-th mode and *j*-th measurement point to the sum of all root mean squares of considered modal responses, as shown in Equation (8). Consequently, the number of MPR values obtained is equal to the number of modes multiplied by the number of measurement points, and the sum of all MPR values is equal to one.

$$MPR_i^j = \frac{MRRMS_i^j}{\sum_{i=1}^{n_m}\sum_{j=1}^{n_d} MRRMS_i^j}, \quad i = 1 \; to \; n_m, \quad j = 1 \; to \; n_d \tag{8}$$

Different MPR values can be obtained in accordance with the dynamic response type. When the acceleration was applied as a dynamic response, MPR values for the higher modes were bigger compared to MPR values obtained from velocity and displacement [38,48]. Within the scope of this study, acceleration responses were employed.

Here, the damage identification procedure is carried out using the MPR change percentage set out in Equation (9), where $DMPR$ is the MPR value of the damaged state and $IMPR$ is the MPR value of the initial state.

$$\Delta MPR_i^j = \frac{DMPR_i^j - IMPR_i^j}{IMPR_i^j} \times 100, \quad i = 1 \; to \; n_m, \quad j = 1 \; to \; n_d \tag{9}$$

3. Case Study

In order to assess the efficiency of MPR values in damage identification, a series of numerical and experimental studies was carried out. For this aim, a steel frame model was designed and built.

3.1. Model Design

A simple steel frame model which simulates the dynamic behavior of the building was built in the laboratory. Steel was selected as a building material due to the its unlabored assembly and uniform structural behavior. Figure 5 shows the detail of the model. The rectangular hollow section with dimensions of 40 × 40 × 2 mm was used as a structural profile. Also, the frame model was welded to a base plate with eight holes to obtain the fixed boundary condition.

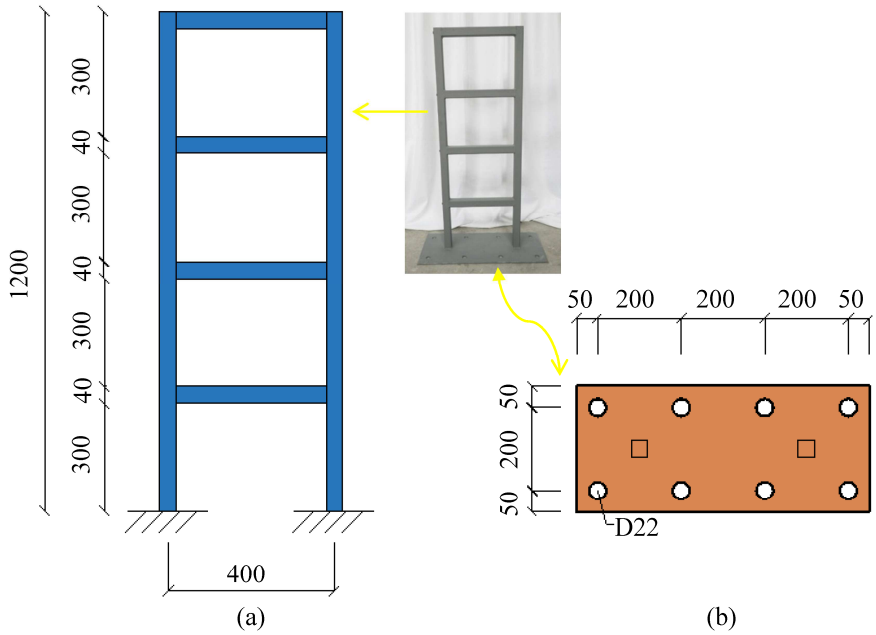


Figure 5. Model detail: (**a**) frame model, (**b**) base plate (dimension in mm).

3.2. Damage Scenarios

The undamaged (as-built) model and eight models with different damage scenarios were provided. The scenarios consisted of single story damage at different story with two severity levels (Figure 6). One can see in Figure 6 that the first-level (level #1) damage was simulated as the removal of a part with 140 mm height and 15 mm width from the middle of the story. The second-level (level #2) damage was simulated by increasing width of the part cut to 20 mm. Finally, these scenarios were employed to evaluate the localization and quantification performance of MPR in the damage identification. This was investigated both numerically and experimentally. Figure 7 shows the frame models of the undamaged, first and second damage scenarios.

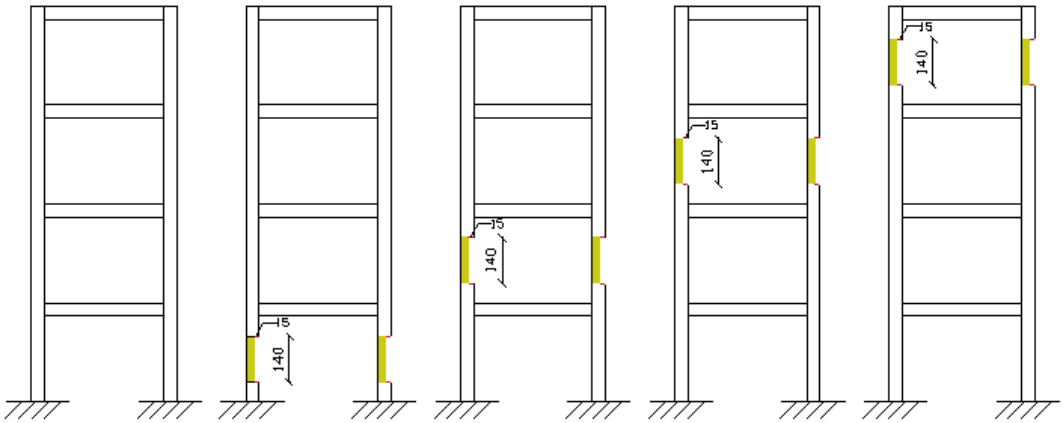


Figure 6. Undamaged model and the first-level damage (level # 1) scenarios.



Figure 7. Undamaged model and damaged models of the first-level damage (yellow ones) and second-level damage (red ones).

3.3. Numerical Study

The FE method was used to calculate the dynamic characteristics of the models. To achieve this, SAP2000 software (2021) [49] was used. The first three in-plane natural frequencies of undamaged and eight damaged models are given in Table 1. Also, the increase/decrease rates of damaged scenarios compared to the undamaged state are given in Table 1. From Table 1, it can be seen that the first natural frequencies were changed between 55.776 Hz and 66.839 Hz. A decrease in natural frequencies occurred after damage. From this, it appears that the most frequency reduction was obtained in second-level damage, where it is located on first story. The reduction was 14.517%. This indicated that the damage located on the first story is more effective on the dynamic response. Figure 8 presents the mode shapes of each model. From Figure 8, it can be seen that there is no notable change in the mode shapes with the damage to model.

Table 1. Comparison of numerical natural frequencies.

Mode	Initial State (Hz)	First Story Damage (Hz)		Second Story Damage (Hz)		Third Story Damage (Hz)		Fourth Story Damage (Hz)	
		Level #1	Level #2	Level #1	Level #2	Level #1	Level #2	Level #1	Level #2
1	65.248	58.878	55.776	64.057	62.666	65.616	65.048	66.723	66.839
2	227.732	209.526	200.864	223.367	221.288	215.512	206.9	223.968	217.989
3	458.989	433.068	421.78	424.473	399.393	450.838	446.798	427.197	404.473
Frequency Variation (%)									
1	0	−9.763	−14.517	−1.825	−3.957	+0.564	−0.307	+2.261	+2.438
2	0	−7.994	−11.798	−1.917	−2.830	−5.366	−9.148	−1.653	−4.278
3	0	−7.514	−10.927	−10.667	−12.984	−6.538	−9.196	−9.029	−11.877

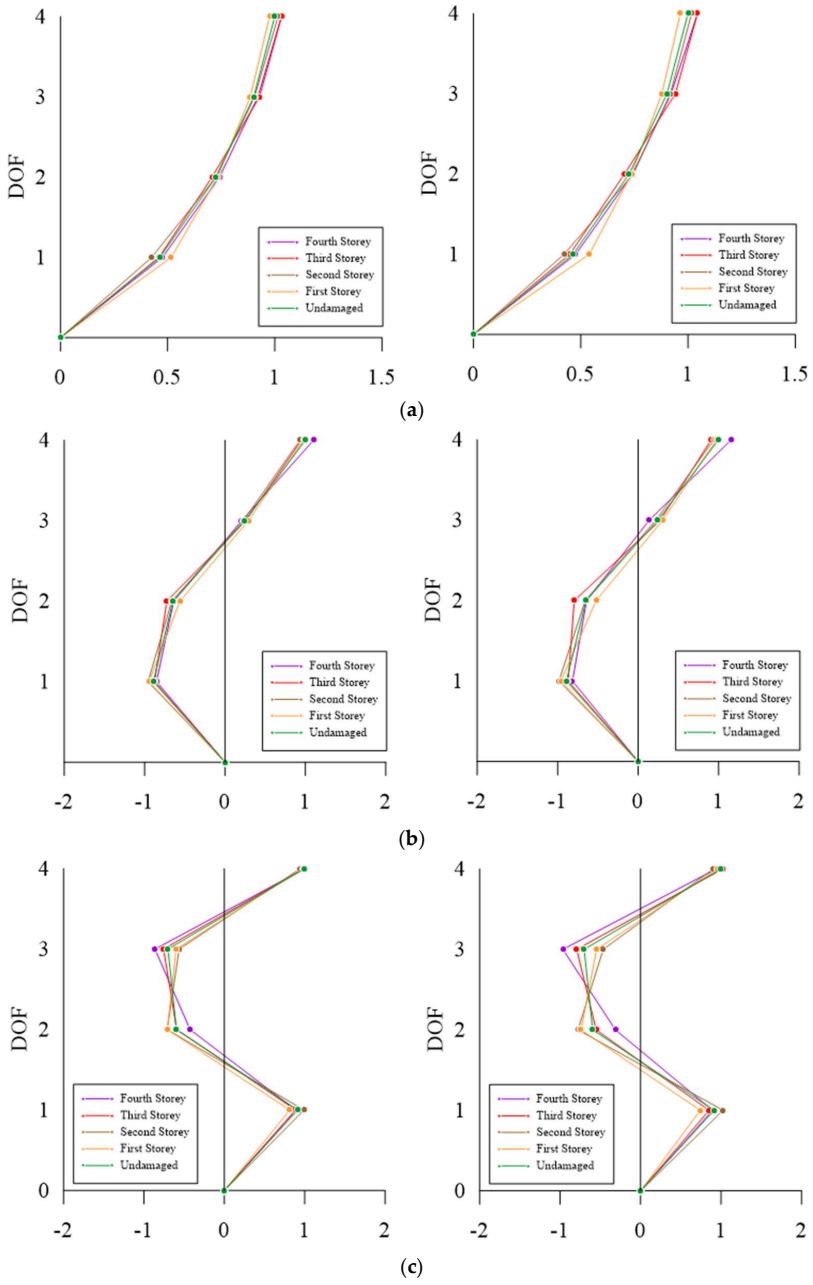


Figure 8. Numerical (**a**) first mode, (**b**) second mode and (**c**) third mode shapes for first- and second-level damages.

The MPR values of the numerical model were derived using band-pass filtering. The user-defined filtering value was assumed to be one. MPR value changes (ΔMPR) caused by level # 1 damage are given in Figure 9. As mentioned earlier, the location of the damage can be obtained using the maximum MPR increase. For instance, in Figure 9a–d, the ΔMPR of damaged DOF are greater, and therefore the estimated damage locations were at the first, second, third and fourth stories, respectively. As can be seen in the Figure, all the location estimations were correct.

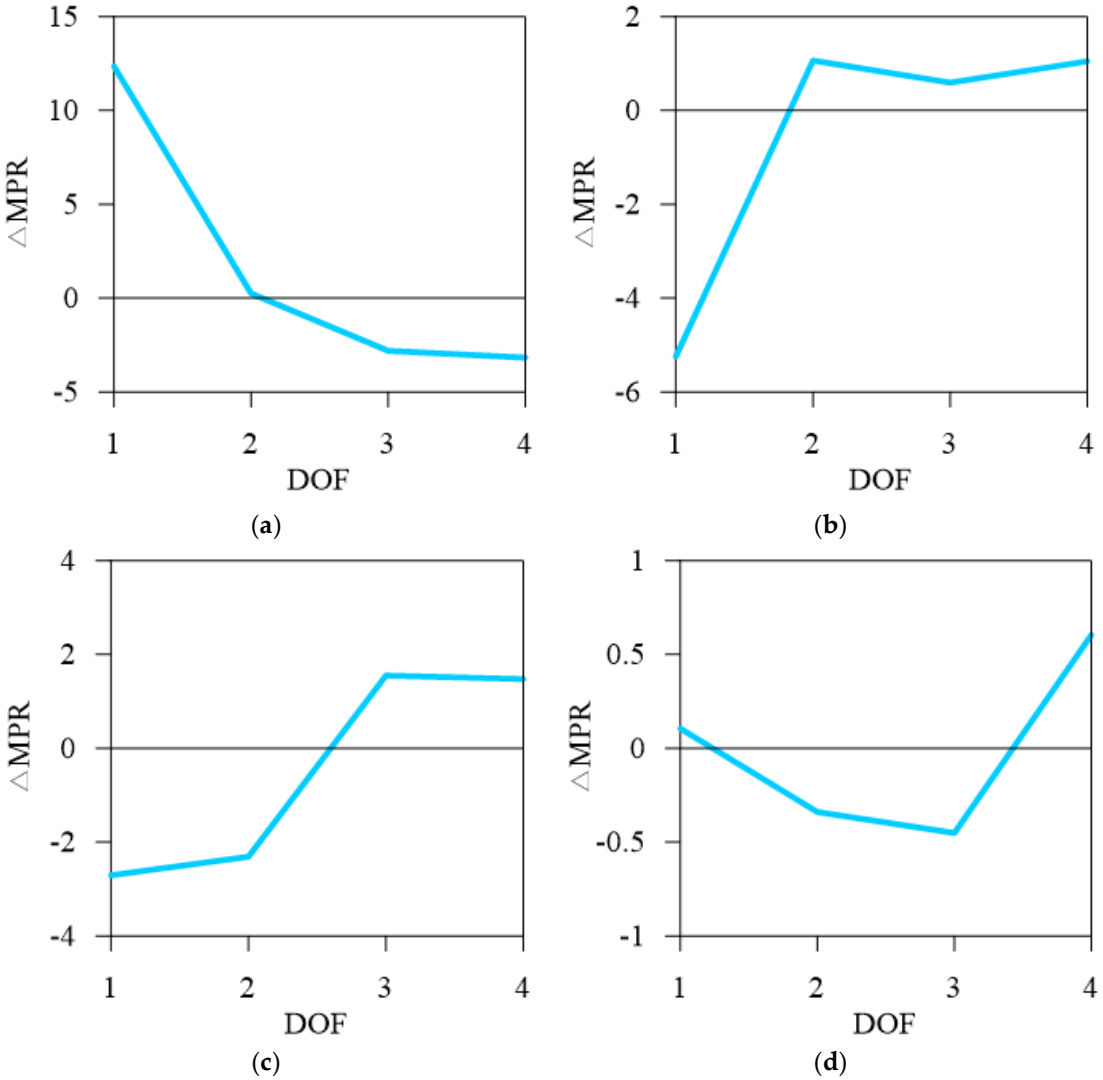


Figure 9. MPR variations obtained from the numerical study for the first-level damage (level #1): (**a**) first story damage, (**b**) second story damage, (**c**) third story damage and (**d**) fourth story damage.

Figure 10 shows the numerical MPR variations obtained from the level #1 damage and level #2 damage scenarios. Using this, the severity of damage was evaluated. As can be seen, the MPR variations changed with the severity of damage. Each ΔMPR value moved further away from the zero axis with the damage of level #2. The conclusion was that the method presented in the study provides an efficient means of damage detection and severity of damage.

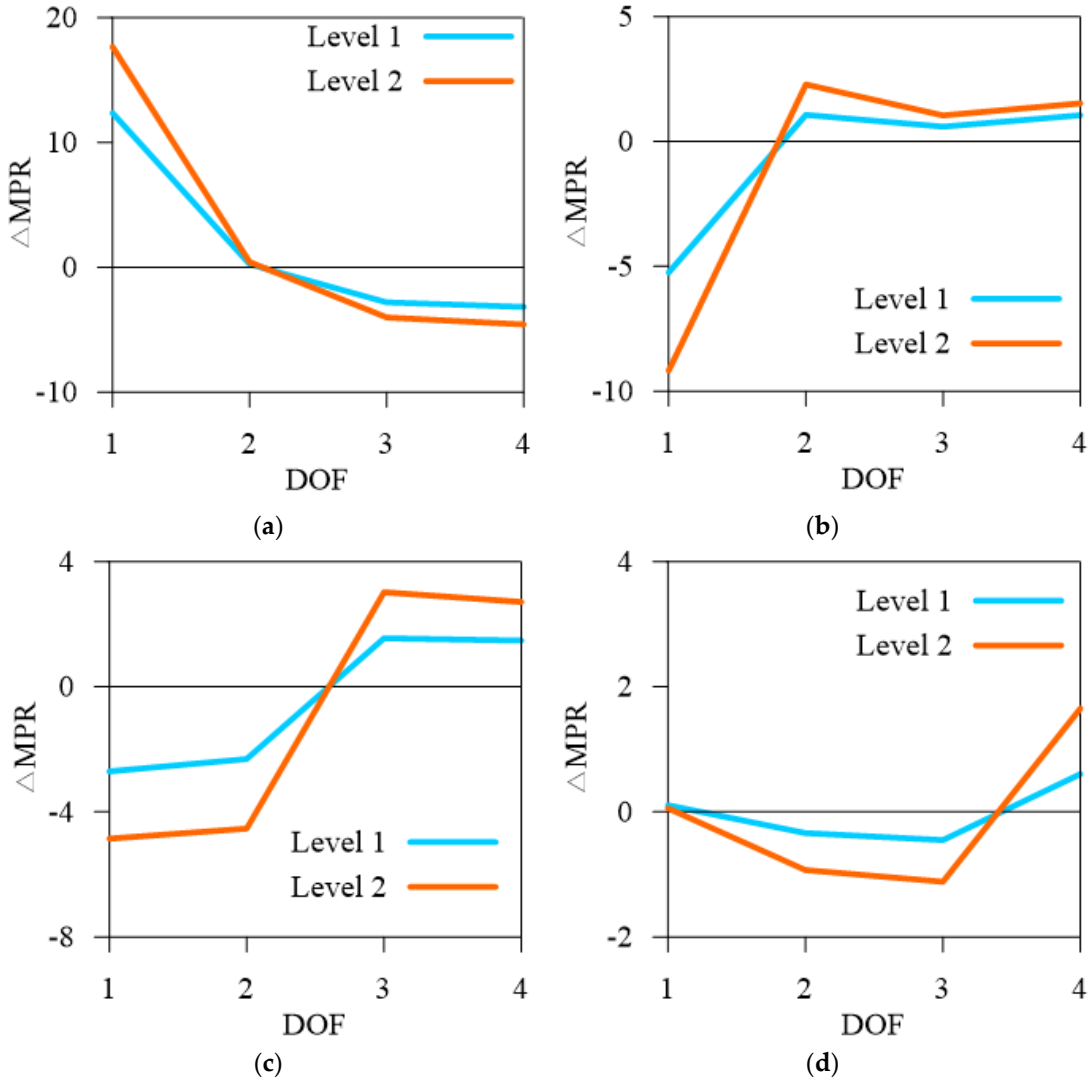


Figure 10. MPR variations obtained from the numerical study for the level #1 and level #2 damage scenarios: (**a**) first story damage, (**b**) second story damage, (**c**) third story damage and (**d**) fourth story damage.

3.4. Experimental Study

The method provided in the study was also evaluated using experimental method. The OMA method was employed to obtain the dynamic response of the models. This method provides effective in monitoring dynamic response, particularly during and after any damage to structures. The test equipment used in the ambient vibration test consisted of: B&K 3053 data acquisition system, B&K 4507 type uni-axial accelerometer and uni-axial signal cables. The accelerometer has a sensitivity of 1 V/g and an operational frequency range of 0.4–6000 Hz. The Nyquist frequency was set to 2048 Hz for experimental study. The accelerometers were placed on the models in the longitudinal direction to measure in-plane dynamic responses, as shown in Figure 11.

Dynamic responses of each model were operated for 10 min, and data were collected in the data acquisition system. Then, the data were processed using BK Connect (2021) software [50]. Lastly, dynamic characteristics such as natural frequency, mode shape and damping ratio of each model were obtained using OMA (2021) software [51]. Figure 12 shows the measurement setup. More information about the experimental setup and equipment is presented in Yilmaz (2022) [43].

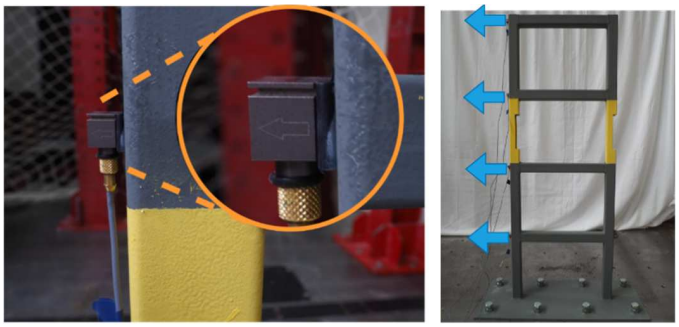


Figure 11. Accelerometer layout on the models.



Figure 12. Photographs from the measurement setup.

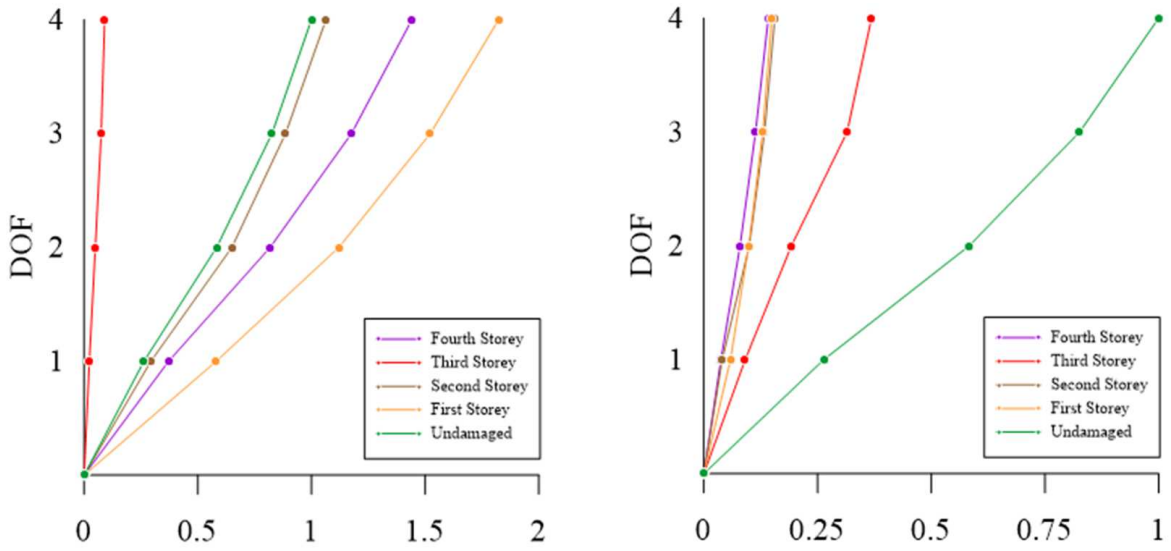
To extract the dynamic characteristics, the EFDD method was employed. The natural frequencies and damping ratios obtained for the undamaged and damaged models are given in Tables 2 and 3, respectively. As can be seen, the first three natural frequencies changed between 67.958 and 459.544 Hz for the undamaged model while the natural frequencies changed between 58.66 and 377 Hz for the damaged models. In addition, and as expected, the natural frequencies decreased (with a maximum variation of 17%) as a result of the introduction of the damage to models. It should be stated, however, that the natural frequencies increased after the introduction of the damage in some scenarios. Therefore, damage identification solely through natural frequency is not practicable in this case. From Table 3, it can be seen that the damping ratios generally have an increasing trend in the case of damaged models. Figure 13 shows the mode shapes of each model. As shown, there was no significant change in mode shapes after introduction of damage.

Table 2. Comparison of experimental natural frequencies.

Mode	Initial State (Hz)	First Story Damage (Hz)		Second Story Damage (Hz)		Third Story Damage (Hz)		Fourth Story Damage (Hz)	
		Level #1	Level #2	Level #1	Level #2	Level #1	Level #2	Level #1	Level #2
1	67.958	61.911	58.66	60.955	59.674	66.676	64.868	68.164	68.059
2	231.753	212.612	200.018	224.117	224.004	216.299	208.044	224.424	210.393
3	459.544	425.015	409.331	410.526	377.608	429.5	417.284	418.054	385.829
Frequency Variation (%)									
1	0	−8.808	−13.682	−10.305	−12.190	−1.886	−4.547	+0.303	+0.149
2	0	−8.259	−13.693	−3.295	−3.344	−6.668	−10.230	−3.162	−9.217
3	0	−7.514	−10.927	−10.667	−17.830	−6.538	−9.196	−9.029	−16.041

Table 3. Comparison of damping ratios.

Mode	Initial State (%)	First Story Damage (%)		Second Story Damage (%)		Third Story Damage (%)		Fourth Story Damage (%)	
		Level #1	Level #2	Level #1	Level #2	Level #1	Level #2	Level #1	Level #2
1	2.943	3.536	4.088	3.699	3.715	3.295	3.464	2.938	2.897
2	0.972	1.034	0.991	0.954	0.936	1.022	1.022	1.003	1.103
3	0.505	0.533	0.542	0.571	0.625	0.551	0.554	0.507	0.579
Damping Ratio Variation (%)									
1	0	+20.15	+38.906	+25.688	+26.232	+11.961	+17.703	−0.17	−1.563
2	0	+6.379	+1.955	−1.852	−3.704	+5.144	+5.144	+3.189	+13.477
3	0	+5.545	+7.327	+13.069	+23.762	+9.109	+9.703	+0.396	+14.653



(**a**)

Figure 13. *Cont*.

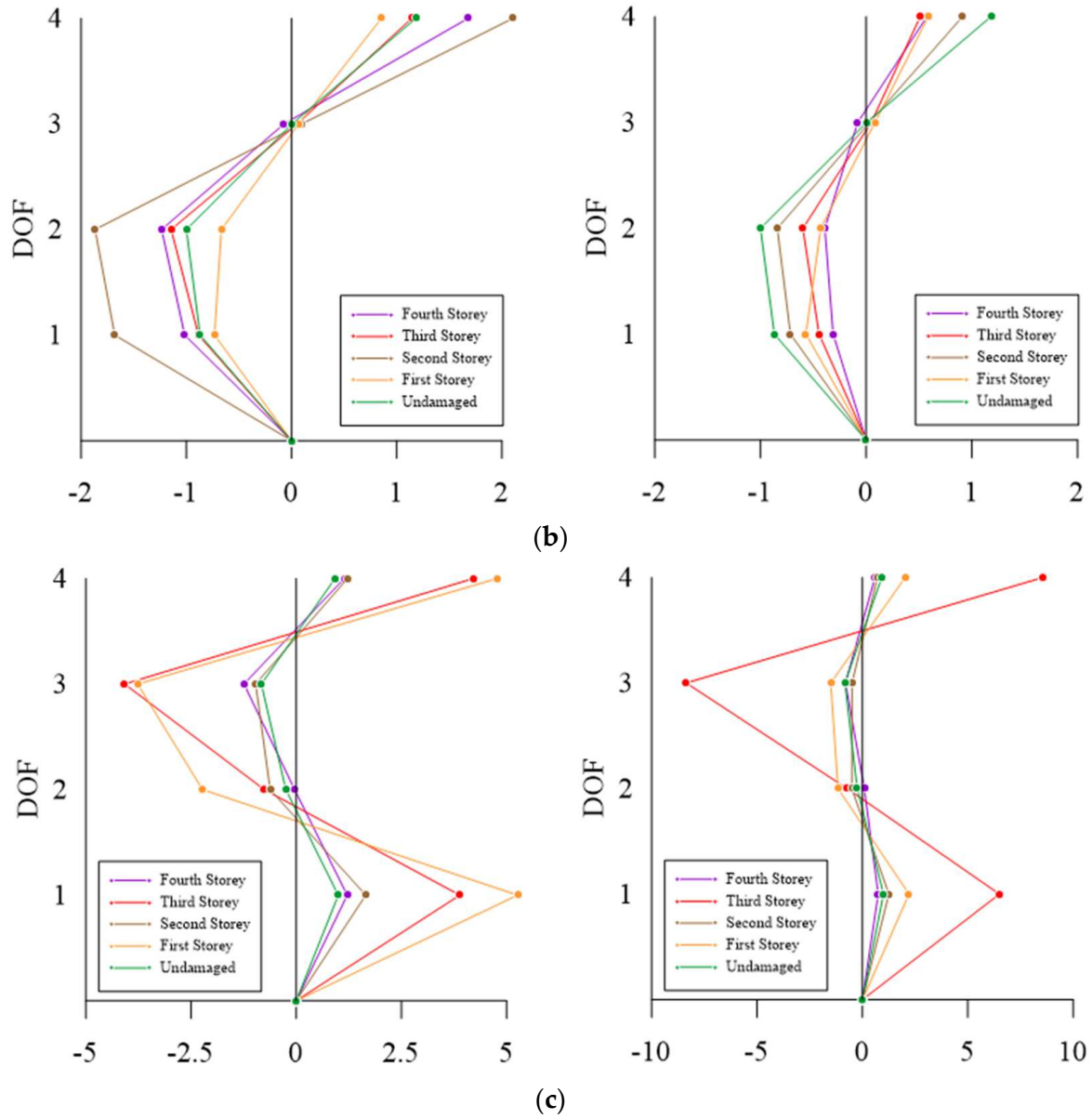


Figure 13. Experimental (**a**) first mode, (**b**) second mode and (**c**) third mode shapes for first- and second-level damages.

The data obtained from the OMA method was used in the MPR derivation method; however, the filtering procedure used in numerical approach was inefficient. Figure 14 shows the MPR variation for each story damage scenario. A user-defined γ value requires in-depth knowledge of both structure and environmental conditions to be sure if that interval is proving the correct variation for damage identification.

Therefore, a more determinate filtering method through MAC rejection level was employed. The method utilizes intervals provided by different MAC rejection levels to determine a definite filtering range. It was concluded that a smaller filtering range derived from a high MAC rejection level was necessary to obtain more precise MPR values. Since a smaller filtering range excludes more data, it was easier to get rid of noisy data caused by environmental conditions. However, a small filtering range requires precise determination of mode frequency.

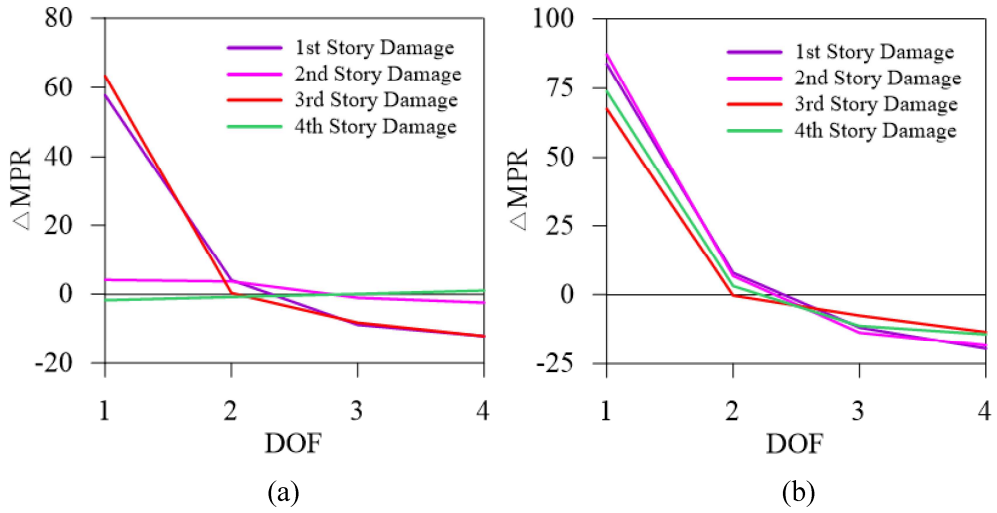


Figure 14. MPR variations in (**a**) first-level damage (level # 1) and (**b**) second-level damage (level # 2) using bandpass filter.

$x_{i(min)}$, $x_{i(max)}$ and x_l values set out in Equation (4) were calculated for 0.4–0.9 MAC rejection levels. Tables 4 and 5 present the filtering values used.

Figure 15a shows the frequency domain data obtained from acceleration readings from the first DOF of the first story in second-level damage. Also, the frequency domain data obtained by filtering with the first mode value is shown in Figure 15b. The filtering is performed using the x_l value calculated from the interval provided by the 0.9 MAC rejection level.

MPR variations in first- and second-level damage scenarios with different x_l values derived from different MAC rejection levels are shown in Figures 16 and 17, respectively. As can be seen, the MAC rejection level of 0.9 provides more reliable estimation of ΔMPR values (see Figures 16c and 17b–d). Therefore, ΔMPR values calculated through the 0.9 MAC rejection level was selected for damage identification. Moreover, one can notice from Figures 16 and 17 that the location estimation for the damage was clearly obtained.

Table 4. MAC rejection levels and their corresponding filtering values for undamaged and first-level damage.

Structural State	Filtering Parameters	MAC Rejection Values					
		0.4	**0.5**	**0.6**	**0.7**	**0.8**	**0.9**
Undamaged	$x_{1(min)}$ (Hz)	32	36	44	52	56	64
	$x_{1(max)}$ (Hz)	104	100	92	84	80	72
	x_l	0.52912	0.47026	0.35254	0.23482	0.17596	0.05824
First Story Damage	$x_{1(min)}$ (Hz)	28	32	40	44	52	56
	$x_{1(max)}$ (Hz)	92	88	80	76	68	64
	x_l	0.486	0.4214	0.29218	0.22757	0.09835	0.03374
Second Story Damage	$x_{1(min)}$ (Hz)	28	32	40	44	52	56
	$x_{1(max)}$ (Hz)	92	88	80	76	68	64
	x_l	0.50931	0.44369	0.31244	0.24682	0.11558	0.04995
Third Story Damage	$x_{1(min)}$ (Hz)	32	40	44	52	56	64
	$x_{1(max)}$ (Hz)	104	96	92	84	80	72
	x_l	0.52007	0.40008	0.34009	0.22011	0.16012	0.04013
Fourth Story Damage	$x_{1(min)}$ (Hz)	32	40	44	52	56	64
	$x_{1(max)}$ (Hz)	104	96	92	84	80	72
	x_l	0.52573	0.40837	0.34969	0.23232	0.17364	0.05628

Table 5. MAC rejection levels and their corresponding filtering values for second-level damage.

Structural State	Filtering Parameters	MAC Rejection Values					
		0.4	**0.5**	**0.6**	**0.7**	**0.8**	**0.9**
First Story Damage	$x_{1(min)}$ (Hz)	32	40	44	48	52	56
	$x_{1(max)}$ (Hz)	88	80	76	72	68	64
	x_l	0.45448	0.3181	0.24991	0.18173	0.11354	0.04535
Second Story Damage	$x_{1(min)}$ (Hz)	36	40	44	48	52	56
	$x_{1(max)}$ (Hz)	84	80	76	72	68	64
	x_l	0.39672	0.32969	0.26266	0.19563	0.1286	0.06157
Third Story Damage	$x_{1(min)}$ (Hz)	36	40	48	52	56	60
	$x_{1(max)}$ (Hz)	92	88	80	76	72	68
	x_l	0.41826	0.3566	0.23327	0.17161	0.10995	0.04828
Fourth Story Damage	$x_{1(min)}$ (Hz)	44	48	52	60	60	64
	$x_{1(max)}$ (Hz)	92	88	84	76	76	72
	x_l	0.35177	0.293	0.23422	0.11668	0.11668	0.05791

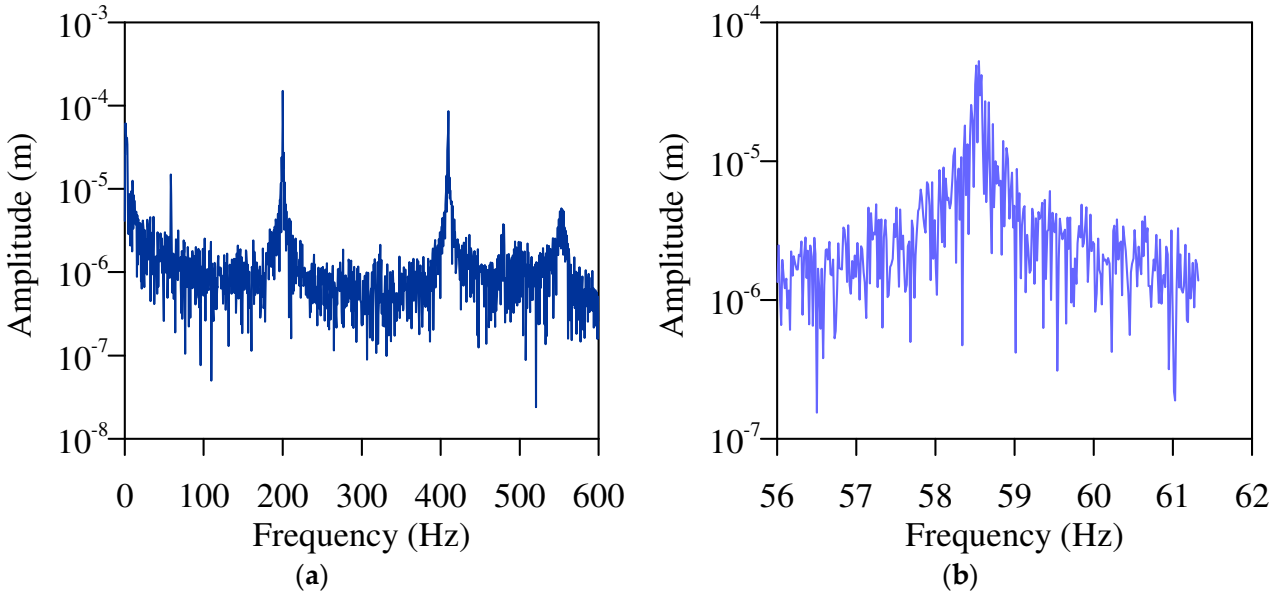


Figure 15. Graph of (**a**) frequency domain data and (**b**) the filtered first mode data of the first story in second-level damage.

Figure 18 presents the experimental MPR variations obtained from the level # 1 damage and level # 2 damage scenarios. As can be clearly seen, the MPR values increased with the damage severity. In other words, an increase in the damage severity was highly effective on the increase in the MPR value of the damaged DOF. Finally, it was concluded that damage localization was possible for each damage scenario, and damage quantification was available for all damage scenarios.

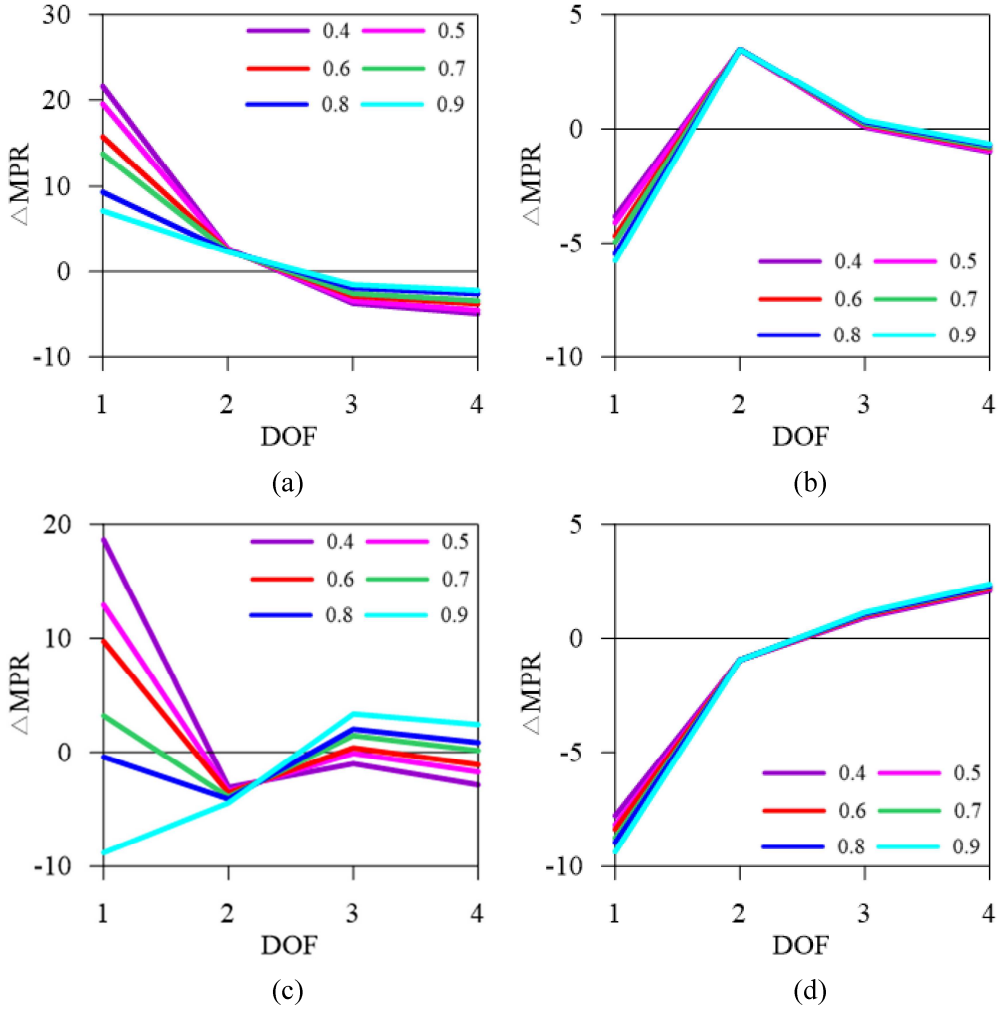


Figure 16. MPR variations in first-level damage (level # 1) with different x_l values derived from different MAC rejection levels: (**a**) first story damage, (**b**) second story damage, (**c**) third story damage and (**d**) fourth story damage.

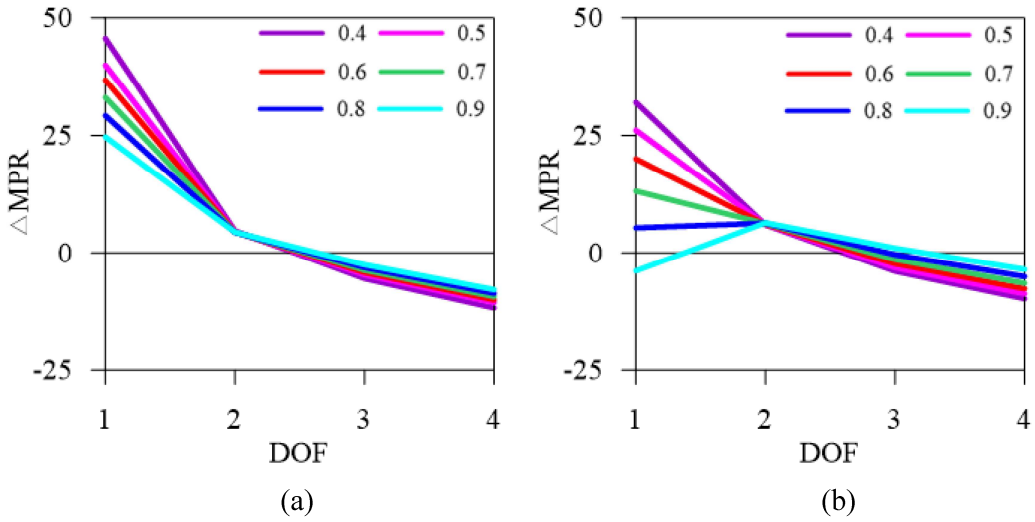


Figure 17. *Cont.*

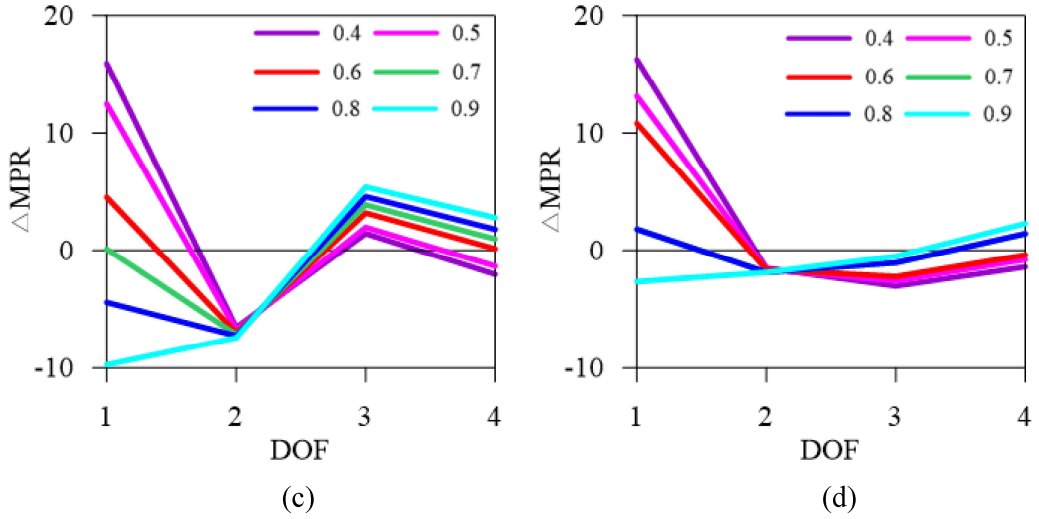


Figure 17. MPR variations in second-level damage (level # 2) with different x_l values derived from different MAC rejection levels: (**a**) first story damage, (**b**) second story damage, (**c**) third story damage and (**d**) fourth story damage.

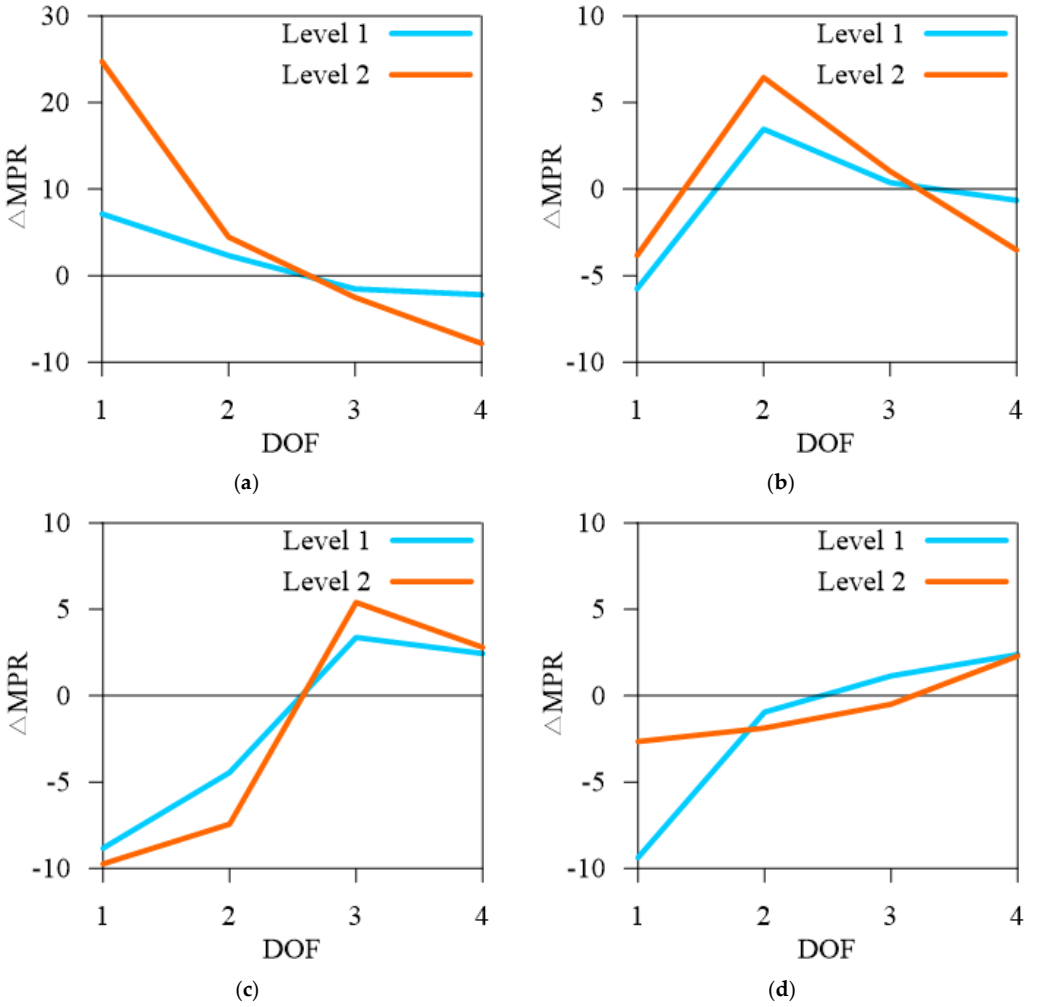


Figure 18. MPR variations obtained from the experimental study for the level # 1 and level # 2 damage scenarios: (**a**) first story damage, (**b**) second story damage, (**c**) third story damage and (**d**) fourth story damage.

4. Conclusions

The usage of the MPR values in damage identification was evaluated using numerical and experimental methods. The identification of damage severity was also evaluated. Eight damage scenarios were introduced for the damage identification of first and second damage levels at different stories. The calculations of MPR values for each damage scenario were detailed to illustrate the efficiency of the proposed method on the damage identification. From the study, the following conclusions can be drawn:

- ✓ The natural frequencies decreased as a result of introduced damage to building model. It should be noted that it is expected to see a decrease in natural frequency upon damage in the system, considering its effect on stiffness, alterations in mass distribution, damping effects and loss of structural integrity. It should be stated, however, that the natural frequencies increased after the introduction of the damage at fourth story. Damping ratios generally increased in the case of damaged models. However, a favorable interpretation was not possible for damage identification.
- ✓ Further study is required for mode shape variation, since the changes in nodal displacements are not observable due to the introduced damage scenarios. The relation between nodal displacements within the mode shape is required. However, using multiple parameters along with mode shape for detecting the damage presence, severity and location can be more effective.
- ✓ The numerical and experimental results indicated that the ΔMPR values were highly capable of detecting the damage location and damage severity.
- ✓ The proposed filtering procedure called "MAC rejection level" provided more acceptable results for the calculating of MPR values during the damage identification procedure. The MAC rejection level can be taken as 0.9.

Finally, based on the results of this study, it is concluded that the MPR variation is a very useful tool for identification structural damage and quantifying damage. This was validated in both numerical and experimental methods. It should be stated, however, that this method requires knowledge about the initial condition of the structures investigated due to the comparative approach during the procedure. Moreover, the filtering method (MAC rejection level) described in this study can be adopted for structural health monitoring to determine rapid or long-term changes in the structural state. A future research stream, which deserves dedicated studies but is out of the scopes of the present study, will be an extensive numerical and experimental investigation on the usage of MPR values for the damage identification in the case of damage to each story of the building.

Author Contributions: Conceptualization, M.G.; Software, Z.Y. and F.Y.O.; Validation, F.Y.O.; Formal analysis, Z.Y. and F.Y.O.; Writing—original draft, M.G.; Writing—review & editing, A.C.A.; Visualization, M.G.; Supervision, A.C.A.; Project administration, A.C.A. All authors have read and agreed to the published version of the manuscript.

Funding: This research has been supported by the Karadeniz Technical University under Research Grant No: FHD-2022-10402.

Data Availability Statement: The datasets generated and/or analyzed during the current study are available from the corresponding author on reasonable request.

Conflicts of Interest: The authors declare no conflict of interest.

References

1. Vandiver, J.K. Structural evaluation of fixed offshore platforms. Ph.D. Dissertation, Massachusetts Institute of Technology, Cambridge, MA, USA, 1975.
2. Adams, R.D.; Cawley, P.; Pye, C.J.; Stone, B.J. A vibration technique for non-destructively assessing the integrity of structures. *J. Mech. Eng. Sci.* **1978**, *20*, 93–100. [CrossRef]
3. Cawley, P.; Adams, R.D. The location of defects in structures from measurements of natural frequencies. *J. Strain Anal. Eng. Des.* **1979**, *14*, 49–57. [CrossRef]

4. Ju, F.D.; Mimovich, M.E. Experimental diagnosis of fracture damage in structures by the modal frequency method. *J. Vib. Acoust.* **1988**, *110*, 456–463. [CrossRef]
5. Lee, Y.-S.; Chung, M.-J. A study on crack detection using eigenfrequency test data. *Comput. Struct.* **2000**, *77*, 327–342. [CrossRef]
6. Rizos, P.; Aspragathos, N.; Dimarogonas, A. Identification of crack location and magnitude in a cantilever beam from the vibration modes. *J. Sound Vib.* **1990**, *138*, 381–388. [CrossRef]
7. Stubbs, N.; Kim, J.T.; Farrar, C.R. Field verification of a nondestructive damage localization and severity estimation algorithm. In *Proceedings-SPIE the International Society for Optical Engineering*; SPIE International Society for Optical: Bellingham, WA, USA, 1995; p. 210.
8. Kam, T.-Y.; Lee, T.Y. Detection of cracks in structures using modal test data. *Eng. Fract. Mech.* **1992**, *42*, 381–387. [CrossRef]
9. Wolff, T.; Mark, R. Fault detection in structures from changes in their modal parameters. In Proceedings of the 7th International Modal Analysis Conference, Las Vegas, NV, USA, 30 January–2 February 1989; Volume 1, pp. 87–94.
10. Yuen, M.M.F. A numerical study of the eigenparameters of a damaged cantilever. *J. Sound Vib.* **1985**, *103*, 301–310. [CrossRef]
11. Pandey, A.K.; Biswas, M.; Samman, M.M. Damage detection from changes in curvature mode shapes. *J. Sound Vib.* **1991**, *145*, 321–332. [CrossRef]
12. Prime, M.B.; Shevitz, D.W. *Linear and Nonlinear Methods for Detecting Cracks in Beams*; No. LA-UR-95-4008; CONF-960238-10; Los Alamos National Lab. (LANL): Los Alamos, NM, USA, 1995.
13. Razak, H.A.; Choi, F.C. The effect of corrosion on the natural frequency and modal damping of reinforced concrete beams. *Eng. Struct.* **2001**, *23*, 1126–1133. [CrossRef]
14. Srinivasan, M.G.; Kot, C.A. *Effect of Damage on the Modal Parameters of a Cylindrical Shell*; No. ANL/CP-74111; CONF-920234-3; Argonne National Lab.: Lemont, IL, USA, 1992.
15. Salawu, O.S.; Clive, W. Bridge assessment using forced-vibration testing. *J. Struct. Eng.* **1995**, *121*, 161–173. [CrossRef]
16. Nikolakopoulos, P.G.; Katsareas, D.E.; Papadopoulos, C.A. Crack identification in frame structures. *Comput. Struct.* **1997**, *64*, 389–406. [CrossRef]
17. Ovanesova, A.V.; Luis, E.S. Applications of wavelet transforms to damage detection in frame structures. *Eng. Struct.* **2004**, *26*, 39–49. [CrossRef]
18. Curadelli, R.O.; Riera, J.D.; Ambrosini, D.; Amani, M.G. Damage detection by means of structural damping identification. *Eng. Struct.* **2008**, *30*, 3497–3504. [CrossRef]
19. Radzieński, M.; Marek, K.; Magdalena, P. Improvement of damage detection methods based on experimental modal parameters. *Mech. Syst. Signal Process.* **2011**, *25*, 2169–2190. [CrossRef]
20. Altunışık, A.C.; Fatih, Y.O.; Sebahat, K.; Volkan, K. Vibration-based damage detection in beam structures with multiple cracks: Modal curvature vs. modal flexibility methods. *Nondestruct. Test. Eval.* **2019**, *34*, 33–53. [CrossRef]
21. Yu, Y.; Wang, C.; Gu, X.; Li, J. A novel deep learning-based method for damage identification of smart building structures. *Struct. Health Monit.* **2019**, *18*, 143–163. [CrossRef]
22. Khodabandehlou, H.; Gökhan, P.; Fadali, M.S. Vibration-based structural condition assessment using convolution neural networks. *Struct. Control. Health Monit.* **2019**, *26*, e2308. [CrossRef]
23. Pandey, A.K.; Biswas, M. Damage detection in structures using changes in flexibility. *J. Sound Vib.* **1994**, *169*, 3–17. [CrossRef]
24. Liew, K.M.; Quan, W. Application of wavelet theory for crack identification in structures. *J. Eng. Mech.* **1998**, *124*, 152–157. [CrossRef]
25. Mehrjoo, M.; Naser, K.; Moharrami, H.; Bahreininejad, A. Damage detection of truss bridge joints using Artificial Neural Networks. *Expert Syst. Appl.* **2008**, *35*, 1122–1131. [CrossRef]
26. Pawar, P.M.; Reddy, K.V.; Ganguli, R. Damage detection in beams using spatial Fourier analysis and neural networks. *J. Intell. Mater. Syst. Struct.* **2007**, *18*, 347–359. [CrossRef]
27. Huang, M.-S.; Gül, M.; Zhu, H.-P. Vibration-based structural damage identification under varying temperature effects. *J. Aerosp. Eng.* **2018**, *31*, 04018014. [CrossRef]
28. Altunişik, A.C.; Genç, A.F.; Günaydin, M.; Okur, F.Y.; Karahasan, O.Ş. Dynamic response of a historical armory building using the finite element model validated by the ambient vibration test. *J. Vib. Control.* **2018**, *24*, 5472–5484. [CrossRef]
29. Altunisik, A.C.; Karahasan, O.S.; Okur, F.Y.; Kalkan, E.; Ozgan, K. *Finite Element Model Updating and Dynamic Analysis of a Restored Historical Timber Mosque Based on Ambient Vibration Tests*; ASTM International: West Conshohocken, PA, USA, 2019.
30. Altunişik, A.C.; Genç, A.F.; Günaydin, M.; Adanur, S.; Yesevi Okur, F. Ambient vibration-based system identification of a medieval masonry bastion for health assessment using nonlinear analyses. *Int. J. Nonlinear Sci. Numer. Simul.* **2018**, *19*, 107–124. [CrossRef]
31. Okur, E.K.; Altunışık, A.C.; Okur, F.Y.; Meral, M.; Yilmaz, Z.; Günaydin, M.; Genç, A.F. Dynamic response of a traditional hımış mansion using updated FE model with operational modal testing. *J. Build. Eng.* **2021**, *43*, 103060. [CrossRef]
32. Luo, J.; Huang, M.; Xiang, C.; Lei, Y. Bayesian damage identification based on autoregressive model and MH-PSO hybrid MCMC sampling method. *J. Civ. Struct. Health Monit.* **2022**, *12*, 361–390. [CrossRef]
33. Soleimani-Babakamali, M.H.; Soleimani-Babakamali, R.; Nasrollahzadeh, K.; Avci, O.; Kiranyaz, S.; Taciroglu, E. Zero-shot transfer learning for structural health monitoring using generative adversarial networks and spectral mapping. *Mech. Syst. Signal Process.* **2023**, *198*, 110404. [CrossRef]
34. Huang, M.; Lei, Y.; Li, X.; Gu, J. Damage identification of bridge structures considering temperature variations-based SVM and MFO. *J. Aerosp. Eng.* **2021**, *34*, 04020113. [CrossRef]

35. Luo, J.; Huang, M.; Xiang, C.; Lei, Y. A Novel Method for Damage Identification Based on Tuning-Free Strategy and Simple Population Metropolis–Hastings Algorithm. *Int. J. Struct. Stab. Dyn.* **2023**, *23*, 2350043. [CrossRef]
36. Malekghaini, N.; Ghahari, F.; Ebrahimian, H.; Bowers, M.; Ahlberg, E.; Taciroglu, E. A Two-Step FE Model Updating Approach for System and Damage Identification of Prestressed Bridge Girders. *Buildings* **2023**, *13*, 420. [CrossRef]
37. Mehboob, S.; Zaman Khan, Q.U.; Ahmad, S. Numerical study for evaluation of a vibration based damage index for effective damage detection. *Bull. Pol. Acad. Sci. Tech. Sci.* **2020**, *68*, 1443–1456.
38. Park, H.S.; Oh, B.K. Damage detection of building structures under ambient excitation through the analysis of the relationship between the modal participation ratio and story stiffness. *J. Sound Vib.* **2018**, *418*, 122–143. [CrossRef]
39. Park, H.S.; Kim, J.; Oh, B.K. Model updating method for damage detection of building structures under ambient excitation using modal participation ratio. *Measurement* **2019**, *133*, 251–261. [CrossRef]
40. Heylen, W.; Stefan, L.; Paul, S. *Modal Analysis Theory and Testing*; Katholieke Universiteit Leuven: Leuven, Belgium, 1997; Volume 200.
41. Brincker, R.; Zhang, L.; Andersen, P. Modal identification from ambient responses using frequency domain decomposition. In Proceedings of the 18th International Modal Analysis Conference (IMAC), San Antonio, TX, USA, 7–10 February 2000; Volume 1, pp. 625–630.
42. Bin Zahid, F.; Ong, Z.C.; Khoo, S.Y. A review of operational modal analysis techniques for in-service modal identification. *J. Braz. Soc. Mech. Sci. Eng.* **2020**, *42*, 398. [CrossRef]
43. Yilmaz, Z. Numerical and Experimental Study of Damage Identification Using Modal Participation Ratio: Detection, Localization and Quantification of Several Damage Scenarios. Master's Thesis, Karadeniz Technical University, Trabzon, Turkey, 2022.
44. Oppenheim, A.V.; Buck, J.R.; Schafer, R.W. *Discrete-Time Signal Processing*; Prentice Hall: Upper Saddle River, NJ, USA, 2001; Volume 2.
45. Jacobsen, N.-J.; Andersen, P.; Brincker, R. Using enhanced frequency domain decomposition as a robust technique to harmonic excitation in operational modal analysis. In Proceedings of the ISMA2006: International Conference on Noise & Vibration Engineering, Heverlee, Belgium, 18–20 September 2006; Katholieke Universiteit: Leuven, Belgium, 2006.
46. Batel, M. Operational modal analysis-another way of doing modal testing. *Sound Vib.* **2002**, *36*, 22–27.
47. Rainieri, C.; Fabbrocino, G.; Cosenza, E. Automated Operational Modal Analysis as structural health monitoring tool: Theoretical and applicative aspects. In *Key Engineering Materials*; Trans Tech Publications Ltd.: Stafa-Zurich, Switzerland, 2007; Volume 347, pp. 479–484.
48. Yilmaz, Z.; Okur, F.Y.; Gunaydin, M.; Altunişik, A.C. Modal participation ratio in damage identification of building structures: A numerical validation. *J. Vib. Control.* **2023**. [CrossRef]
49. Computers and Structures Inc. *SAP2000. V.21*; CSI. PC: Walnut Creek, CA, USA, 2021.
50. Brüel & Kjær Sound & Vibration Measurement. *BK Connect, V. 25.1*; B&K. PC: North Denmark, Denmark, 2021.
51. Brüel & Kjær Sound & Vibration Measurement. *PULSE Operational Modal Analysis, V. 7.1*; B&K. PC: North Denmark, Denmark, 2021.

Disclaimer/Publisher's Note: The statements, opinions and data contained in all publications are solely those of the individual author(s) and contributor(s) and not of MDPI and/or the editor(s). MDPI and/or the editor(s) disclaim responsibility for any injury to people or property resulting from any ideas, methods, instructions or products referred to in the content.